Emission characteristics of water in the Universe

Poelman, Dieter Roel

Chapter 2

β3D, a multi-zone escape probability code

We present a newly developed numerical method and computer code to calculate the radiative transfer and excitation of molecular lines. The use of a multi-zone formalism, in contrast with a one-zone approach, allows to calculate excitation gradients within opaque sources. The level populations in every gridpoint depend on the level populations in all the other gridpoints through the different escape probabilities that connect any two gridpoints. In this way, global information is used to determine iteratively in every gridpoint the ambient level populations. Continuum emission and absorption by dust, known to be an important contributor to the excitation of molecules, e.g., H_2O, is taken into account. We benchmark the code (i) by calculating the excitation of H_2O in a static cloud, (ii) in an expanding sphere, and (iii) by computing the excitation of HCO^+ in an infalling envelope around a protostar. We find that the resulting level populations are in good agreement with existing Monte Carlo and Accelerated Lambda Iteration codes.

Contains parts from Poelman, D.R., & Spaans, M. 2005, A&A, 440, 559-567

2.1 Introduction

Our understanding of astrophysical objects, such as molecular clouds, young stellar objects (YSOs), disks, planetary nebulae and photon dominated regions (PDRs), requires not only observations but also detailed modeling in order to retrieve information on physical parameters, e.g., temperature, density, abundance, velocity structure, and turbulence. Line emission from molecules, such as CO and H_2O, has been observed extensively in the past decades (Federman et al. 1980; Helmich et al. 1996; Ladd et al. 1998; Stark et al. 2004; van Dishoeck 2004) and has been proven to be a powerful tool to reveal the behaviour of the aforementioned environments. Furthermore, molecular line transitions play a key role in tracing the properties of galaxies and their evolution, e.g., molecular line ratios of HNC, HCN, HCO^+, and very high-J CO can distinguish between a starburst or an active galactic nuclei (AGN) activity (Meijerink et al. 2007).

To interpret line emission, line radiative transfer programs are required which calculate accurately the non-LTE (local thermodynamic equilibrium) level populations and the resulting output spectra. The level populations in their turn follow after solving the local statistical equilibrium equations. However, the local solution is coupled to the global radiative transfer equations. In other words, the local level populations are coupled to the global radiation field and hence the global level populations. This feedback of the surrounding level populations on the local ones makes radiative transfer far from straightforward.

One way to model line emission from various molecules is to make use of a one-zone escape probability method, in which the probability β indicates the chance for a photon to escape the cloud in a direct flight without absorption or scattering. The one-zone approach is applied only for isothermal and homogeneous media and has been used in the past to calculate, e.g., the radiative cooling of warm molecular gas (Neufeld & Kaufman 1993), the far-infrared water emission from shock waves (Kaufman & Neufeld 1996) and water maser emission (Neufeld & Melnick 1991). Despite the wide range of applications of this method, other techniques, e.g., Monte Carlo (MC), Accelerated Lambda Iteration (ALI) and Local linearization (MULTI type) codes, that solve non-LTE multi-level radiative transfer problems, were created in order to meet with the non-local effects that arise in certain problems. Monte Carlo codes have been used over the years to study, e.g., masers (Spaans & van Langevelde 1992), ultraviolet (UV) continuum transfer (Spaans 1996) and molecular line transfer (Hogerheijde & van der Tak 2000). These have been proven to be reliable tools. However, they have the disadvantage of having convergence problems at high optical depths, i.e., $\tau \geq 100$.

In this chapter we examine and compare a newly developed radiative transfer code that is used throughout the thesis for modeling the strength

of molecular lines emerging from interstellar regions. The multi-zone component of the method, in contrast with a one-zone approach, enables to calculate locally the equations of statistical equilibrium in different positions in the cloud, taking into account global information.

2.2 Radiative transfer: general

One of the essential quantities in the transfer of radiation is the specific intensity I_ν. It is defined as the energy passing through an infinitesimally small area dA within a solid angle dΩ in time dt and in frequency range dν, i.e.,

$$\mathrm{d}E = I_\nu \mathrm{d}A \mathrm{d}t \mathrm{d}\Omega \mathrm{d}\nu. \tag{2.1}$$

When a ray passes through a medium, its specific intensity can change as energy is added or substracted from it by emission or absorption. To describe the emission of a transition from level i to level j at frequency ν, the spontaneous emission coefficient j_ν is introduced. It is defined as the energy emitted per unit time, per unit solid angle and per unit volume. Since each atom/molecule contributes an energy $h\nu$ distributed over 4π solid angle for each transition, $j_\nu = \frac{h\nu}{4\pi} n_i A_{ij} \varphi(\nu)$, with n_i the population density of the ith level, and A_{ij} the Einstein A-coefficient. The energy difference between two levels is not infinitely sharp and is described by the line profile function $\varphi(\nu)$. Thus, the intensity added to the beam by spontaneous emission traveling over a distance ds is $\mathrm{d}I_\nu = j_\nu \mathrm{d}s$. Conversely, the absorption coefficient α_ν is defined as the energy absorbed out of a beam in frequency range dν per unit time, per unit solid angle and per unit volume, i.e., $\alpha_\nu = \frac{h\nu}{4\pi} n_j B_{ji} \varphi(\nu)$, assuming that the absorption is described with the same line profile function that defines the emission. B_{ji} is the Einstein B-coefficient. However, stimulated emission is not incorporated in this, and is treated as negative absorption. Hence, the absorption coefficient, corrected for stimulated emission, is $\alpha_\nu = \frac{h\nu}{4\pi}(n_j B_{ji} - n_i B_{ij})\varphi(\nu)$. The loss of intensity in a beam as it travels a distance ds can be written as $\mathrm{d}I_\nu = -\alpha_\nu I_\nu \mathrm{d}s$.

It is now possible to describe the behaviour of radiation through a medium. The transfer of radiation is embodied by an equation connecting the emission and absorption properties of the photons passing through the cloud along a distance ds:

$$\frac{\mathrm{d}I_\nu}{\mathrm{d}s} = j_\nu - \alpha_\nu I_\nu. \tag{2.2}$$

Equation 2.2 can be rewritten as

$$\frac{\mathrm{d}I_\nu}{\mathrm{d}\tau_\nu} = S_\nu - I_\nu, \tag{2.3}$$

with τ_ν the optical depth defined as $\mathrm{d}\tau_\nu = \alpha_\nu \mathrm{d}s$ and $S_\nu = j_\nu/\alpha_\nu$ the source function, defined as the ratio of the emission coefficient to the absorption coefficient. As a result

$$S_\nu = \frac{2h\nu_{ij}^3}{c^2}\left[\frac{n_j g_i}{n_i g_j} - 1\right]^{-1}, \tag{2.4}$$

where g_i and g_j are the statistical weights of levels i and j, respectively. The equation of radiative transfer can now be formally solved:

$$I_\nu(\tau) = I_\nu(0)\mathrm{e}^{-\tau_\nu} + \int_0^\tau S_\nu(\tau')\mathrm{e}^{\tau'-\tau}\mathrm{d}\tau'. \tag{2.5}$$

This integral is evaluated along all possible straight lines through the medium. The mean integrated intensity received in a point from all solid angles $\mathrm{d}\Omega$ is then given by

$$\langle J_\nu \rangle = \int_0^\infty \mathrm{d}\nu \varphi_\nu J_\nu \quad \text{with} \quad J_\nu = \frac{1}{4\pi}\int_0^\infty I_\nu \mathrm{d}\Omega. \tag{2.6}$$

Locally, the level populations are determined by collisions and radiation through the equations of statistical equilibrium:

$$n_i(\mathrm{x, y, z})\sum_{j\neq i}^{l} R_{ij}(\mathrm{x, y, z}) = \sum_{j\neq i}^{l} n_j(\mathrm{x, y, z})R_{ji}(\mathrm{x, y, z}), \tag{2.7}$$

where l is the total number of levels included. Since the set of l statistical equilibrium equations is not independent, one equation has to be replaced by the conservation equation, i.e.,

$$n_x = \sum_{j=0}^{l} n_j\,, \tag{2.8}$$

where n_x is the number density of species x in all levels.
$R_{ij}(\mathrm{x, y, z})$ is expressible in terms of the Einstein A- and B-coefficients and the collisional excitation ($i<j$) and de-excitation ($i>j$) rates C_{ij}:

$$R_{ij}(\mathrm{x, y, z}) = \begin{cases} A_{ij} + B_{ij}\langle J_\nu\rangle + C_{ij}(\mathrm{x, y, z}), & i > j \\ B_{ij}\langle J_\nu\rangle + C_{ij}(\mathrm{x, y, z}), & i < j. \end{cases} \tag{2.9}$$

Locally, the equations of statistical equilibrium couple the level populations to each other through the processes indicated by Eq. 2.9. However, this equation can only be solved if $\langle J_\nu\rangle$ is known. Hence, the local equations of statistical equilibrium are coupled globally through the radiation field. In other words, the intensity of spectral lines depends on the level populations,

which in their turn depend on the radiation field. Thus, equations 2.5 – 2.9 form a coupled set of equations.

In general, $\langle J_\nu \rangle$ has contributions from the Cosmic Microwave Background (CMB), the interstellar radiation field (ISRF), dust and spectral lines. One can assume, to first order, when modeling an astrophysical object that the physical conditions within the cloud do not vary much. In this case, $\langle J_\nu \rangle$ can be approximated by the local conditions only. This is the basic principle of the Large Velocity Gradient Method, the Sobolev method, or the one-zone escape probability formalism (e.g., Sobolev 1960; Goldreich and Kwan 1974; de Jong et al. 1980). However, usually temperature and density gradients are present and such simplifications cannot be made. One can solve this set of equations by adopting the ALI or MC method. However, these methods have the disadvantage of slow convergence in highly optically thick regions.

In the following, we present an alternative method to solve the radiative transfer equations that does not suffer from convergence problems at high optical depth and retains the accuracy of previous methods. The code is not limited to spherical symmetric or axisymmetrical problems, in that an unique temperature (gas and dust), density, and abundance value can be attributed to every position in the cloud (see, e.g., Chapter 3 in which high density clumps are randomly distributed within a low density interclump medium).

2.3 Line transfer through a multi-zone escape probability method in a dusty medium

We calculate the transfer of line radiation of an atom/molecule in an (in)homogeneous three-dimensional spherical cloud by use of a multi-zone escape probability method. Consideration of the escape probability from one gridpoint to all the others allows us to calculate locally the radiative transfer but with global information, see Fig. 2.1.
$\langle J_\nu(\mathrm{x, y, z}) \rangle$ is the solid angle averaged, frequency integrated radiation field corresponding to the transition from level i to j with rest frame frequency ν_{ij} at position (x, y, z) in the cloud, given by:

$$\langle J_\nu(\mathrm{x, y, z}) \rangle = (1-\beta_{ij}) S_{ij}(\mathrm{x, y, z}) + (\beta_{ij} - \eta_{ij}) B(\nu_{ij}, T_\mathrm{d}) + \eta_{ij} B(\nu_{ij}, T = 2.7\,\mathrm{K}), \quad (2.10)$$

where $B(\nu_{ij},\, T_\mathrm{d})$ is the infrared emission of dust at a temperature T_d, and $B(\nu_{ij}, T = 2.7\,\mathrm{K})$ the 2.7 K cosmic microwave background (CMB) contribution. Two photon escape probabilities are introduced: (1) β_{ij} is the probability that a photon escapes line absorption:

$$\beta_{ij} = \delta_{ij} + \int_0^\infty \frac{\mathrm{d}\Omega}{4\pi} \int_0^\infty \mathrm{d}\nu \varphi_\nu \frac{\tau_\mathrm{L}}{\tau_\mathrm{L} + \tau_\mathrm{d}} \mathrm{e}^{-(\tau_\mathrm{L} + \tau_\mathrm{d})}, \quad (2.11)$$

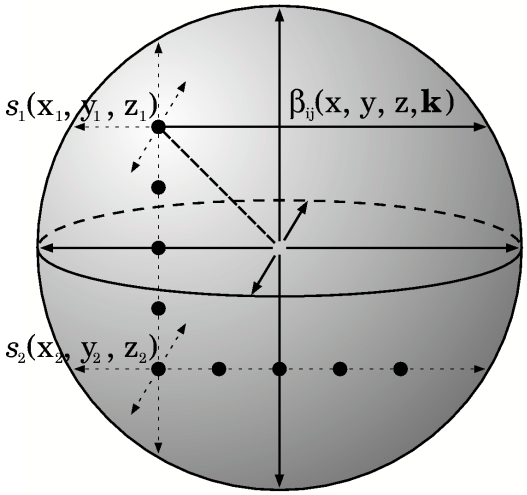

Figure 2.1: Representation of a sphere in which every gridpoint is connected with the neigbouring gridpoints through the different escape probabilities.

where $\tau_{\rm L}$ and $\tau_{\rm d}$ are the line and dust optical depths, respectively, and δ_{ij} is the probability per scattering that a photon will be absorbed by dust (Hummer 1968; Hummer and Rybicki 1970):

$$\delta_{ij} = \int_0^\infty \frac{{\rm d}\Omega}{4\pi} \int_0^\infty {\rm d}\nu \varphi_\nu \frac{\tau_{\rm d}}{\tau_{\rm L} + \tau_{\rm d}}. \tag{2.12}$$

(2) η_{ij} is the probability that a photon escapes dust absorption as well as line absorption, and therefore contributes to the observed line emission by a distant observer:

$$\eta_{ij} = \int_0^\infty \frac{{\rm d}\Omega}{4\pi} \int_0^\infty {\rm d}\nu \varphi_\nu {\rm e}^{-(\tau_{\rm L}+\tau_{\rm d})}. \tag{2.13}$$

Note that the angle dependence in the above equations is replaced in our formalism by the summation over a fixed number of directions, i.e.,

$$\int_0^\infty \frac{{\rm d}\Omega}{4\pi} = \sum_{k=1}^{N} \tag{2.14}$$

The number of directions is arbitrary, but a 6-ray approximation is implemented in 3D, i.e., $N = 6$. This particular number is chosen as it represents the different orthogonal directions in a three-dimensional Cartesian grid. The effect of more directions, e.g., 26 – in which the values −1, 0, or 1 are

assigned to x, y, and z of the k-vectors (x, y, z) – on the converged solution of the level populations is small in comparison with the 6 implemented directions. However, 26 directions lead to more angular resolution, but is by comparison more time consuming by a factor of ~ 6. Many problems in astrophysics, e.g., a static or spherical symmetric infalling cloud, do not require larger angular resolution than is achieved with the 6 implemented directions. Nevertheless, more 'exotic' processes of radiation, such as maser emission, necessitate higher angular resolution, as this intense radiation is confined within small angular sizes with beaming angles in the range of $10^{-1} - 10^{-2}$ rad (Elitzur 1992).

Equations 2.7 – 2.10 constitute the core of the escape probability method that includes dust radiation. Equation 2.10 has the following physical interpretation: the first term on the right-hand side is the contribution of line photons whose number is proportional to the amount of line absorption, $1 - \beta_{ij}$. Similarly, the second term is the contribution of dust photons whose number is proportional to the amount of dust absorption, $\beta_{ij} - \eta_{ij}$. The third term is the amount of external radiation reaching the test point. Consider now an extreme case in which both line and dust optical depths are large in all directions. In this case we obtain

$$\langle J_\nu(\mathrm{x, y, z})\rangle = (1 - \delta_{ij}) S_{ij}(\mathrm{x, y, z}) + \delta_{ij} B(T_\mathrm{d}), \tag{2.15}$$

i.e., the contribution of each component to the total radiation field is determined by the ratio of dust to line optical depths. The dust contribution to the radiation field depends on the line optical depth, and vice versa. In the absence of dust ($\tau_\mathrm{d} = 0$), we obtain the usual expression for the escape probability (cf. Castor 1970; de Jong, Chu, & Dalgarno 1975), i.e.,

$$\beta_{ij}(\mathrm{x, y, z}) = \int_0^\infty \frac{\mathrm{d}\Omega}{4\pi} \left[\frac{1 - \mathrm{e}^{-\tau_\mathrm{L}}}{\tau_\mathrm{L}} \right] = \sum_{k=1}^{N} \left[\frac{1 - \mathrm{e}^{-\tau_\mathrm{L}}}{\tau_\mathrm{L}} \right]. \tag{2.16}$$

Note that the probability for a photon to escape in a point equals the sum of the escape probabilities over all directions, i.e.,

$$\beta_{ij}(\mathrm{x, y, z}) = \sum_{\{\vec{k}\}} \beta_{ij}(\mathrm{x, y, z}, \{\vec{k}\}). \tag{2.17}$$

The optical depth averaged over the line, in direction $\vec{k}$ over a distance $s = s_2(\mathrm{x_2, y_2, z_2}) - s_1(\mathrm{x_1, y_1, z_1})$ is given by

$$\tau_{ij}(\mathrm{x, y, z}, \vec{k}) = \frac{A_{ij} c^3}{8\pi \nu_{ij}^3} \int_{s=s_1}^{s=s_2} \frac{n_i}{\Delta v_\mathrm{D}} \left[\frac{n_j g_i}{n_i g_j} - 1 \right] \mathrm{d}s. \tag{2.18}$$

Note that the optical depth τ_L at position (x, y, z) in the cloud, as used in Eq. 2.11 – 2.13, is the sum of the contributions of optical depths $\tau_{ij}(\mathrm{x, y, z}, \vec{k})$

from the starting point (x, y, z) up to the edge of the cloud. Hence, the probability for a photon to escape is connected through all the gridpoints along its line of sight. The velocity dispersion, $\Delta v_{\rm D}$, includes thermal and turbulent contributions, i.e., $\Delta v_{\rm D} = (v_{\rm th}^2 + v_{\rm turb}^2)^{1/2}$. Turbulence in, for instance, molecular clouds can be combined with the thermal speed of the gas into a Gaussian distribution. The resultant Doppler profile is

$$\varphi(\nu) = \frac{1}{\Delta\nu_{\rm D}\sqrt{\pi}} {\rm e}^{-(\nu-\nu_0)^2/(\Delta\nu_{\rm D})^2}, \tag{2.19}$$

where the constant $(\Delta\nu_{\rm D}\sqrt{\pi})^{-1}$ is determined by the normalization condition $\int \varphi(\nu){\rm d}\nu = 1$ under the (reasonable) assumption that $\Delta\nu_{\rm D} \ll \nu_0$. The Doppler frequency width $\Delta\nu_{\rm D}$ is given by $\Delta\nu_{\rm D} = \Delta v_{\rm D}\frac{\nu_{ij}}{c}$. Typical line widths range from a few kilometers per second up to a few tens of kilometers per second, far in excess of plausible thermal velocities in the clouds. For reference, the rms thermal velocity of a $^{12}C^{16}O$ molecule at 30 K is 0.16 km s^{-1}. Therefore, in many circumstances, the turbulent dispersion $v_{\rm turb}$ is larger than the thermal velocity $v_{\rm th}$ of the gas and dominates the line broadening in molecular clouds.

The dust optical depth in direction $\vec{k}$ over a distance $s = s_2({\rm x}_2, {\rm y}_2, {\rm z}_2) - s_1({\rm x}_1, {\rm y}_1, {\rm z}_1)$ is calculated as

$$\tau_{\nu,{\rm dust}}({\rm x}, {\rm y}, {\rm z}, \vec{k}) = \int_{s=s_1}^{s=s_2} \kappa_\nu \rho_{\rm dust} {\rm d}s, \tag{2.20}$$

where κ_ν is the dust opacity in cm^{-2} per unit (dust) mass and $\rho_{\rm dust}$ is the mass density of dust. Grain properties throughout the thesis are taken from Ossenkopf & Henning 1994. The dust optical depth $\tau_{\rm d}$ at position (x, y, z) in the cloud, as used in Eq. 2.11 – 2.13, is the sum of the contributions of dust optical depths $\tau_{\nu,{\rm dust}}({\rm x}, {\rm y}, {\rm z}, \vec{k})$ from the gridpoint (x, y, z) up to the edge of the cloud, in analogy with the optical depth in the line.

A converged solution of the set of coupled level populations is found after global iteration. This set of level populations is then used by a ray tracing program to compute line intensities. The intensity of a transition from level i to j ($i > j$) is given by

$$I_{ij,{\rm total}} = \frac{1}{4\pi}\int_0^r \Lambda_{ij,{\rm local}} {\rm d}s, \tag{2.21}$$

with

$$\Lambda_{ij,{\rm local}} = n_i A_{ij} h\nu_{ij}\beta(\tau_{ij})\{[S(\nu_{ij}) - P(\nu_{ij})]/S(\nu_{ij})\}, \tag{2.22}$$

and

$$P(\nu_{ij}) = B(\nu_{ij}, T = 2.7\ {\rm K}) + (1 - {\rm e}^{-\tau_{{\rm dust},\nu_{ij}}})B(\nu_{ij}, T_{\rm d}). \tag{2.23}$$

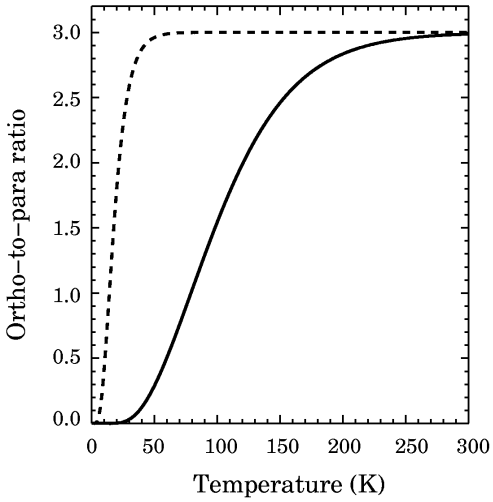

Figure 2.2: Ortho-to-para ratio of H_2 (*solid*) and H_2O (*dash-dotted*) in LTE as a function of the local kinetic temperature.

2.4 Collisional rate coefficients

Because the interpretation of observed lines requires knowledge of the collisional excitation rates responsible for line formation, it is necessary to work with the most accurate collisional rate data available. In this thesis, spectroscopic and collisional input for the modeling is taken from the molecular database by Schöier et al. (2005). In the case of water, the collisional rates are taken from Green et al. (1993) for inelastic collisions between He and H_2O in the temperature range from 140 K to 2000 K. To account for the different reduced mass of the H_2 collisional partner, the rate coefficients are scaled by a factor of 1.348. Rate coefficients of o- and p-H_2O owing to collisions with o- and p-H_2 at kinetic temperatures from 20 K to 140 K are taken from Phillips et al. (1996). In addition, rate coefficients for H_2O in collisions with o-H_2 and p-H_2 for the low temperature regime (5 – 20 K) are taken from Grosjean et al. (2003) and Dubernet & Grosjean (2002), respectively. In general, collisions between molecules and electrons contribute to the total collisional rate. However, this is only the case when the electron abundance, X(e), is high. For instance, using the H_2O-electron collisional rates presented by Faure et al. (2004), we find that the contribution by electrons to the total collisional excitation rate is less than 1% when X(e) is $\sim 10^{-6}$. Only when the electron abundance is of the order of 10^{-5} and higher, does the contribution by electron collisions become equal

to the collisional rates of H_2O with p-H_2, and consequently has to be taken into account. These large electron abundances can be found in regions with strong X-rays, e.g., at the edges of circumstellar disks.
Observational studies of the ortho-to-para ratio (OPR) of H_2 in PDRs have found values in the range of $1.5-2.2$ (Hasegawa et al. 1987; Ramsay et al. 1993; Chrysostomou et al. 1993; Hora & Latter 1996; Shupe et al. 1998), and are not constant because of gas temperature variations within the PDR. However, some of the values found in previously mentioned studies differ slightly from the exact value since only H_2 J=1/J=0 transitions are taken into account. To come to an exact result, all J levels need to be considered. Therefore, we adopt the expression for the OPR in thermal equilibrium defined by

$$\mathrm{OPR}(H_2) = \frac{3\sum_{J=\mathrm{odd}}(2J+1)\exp[-BJ(J+1)/T_\mathrm{L}]}{\sum_{J=\mathrm{even}}(2J+1)\exp[-BJ(J+1)/T_\mathrm{L}]}, \tag{2.24}$$

where n_o and n_p are the abundances of o- and p-H_2, respectively, J the rotational quantum number, B the rotational constant of H_2 ($B = 87.6$ K), and T_L the local temperature. A similar expression holds for the o- and p-H_2O OPR:

$$\mathrm{OPR}(H_2O) = \frac{(2I_\mathrm{o}+1)\sum(2J+1)\exp\left(-\frac{E_\mathrm{o}(J,K_\mathrm{a},K_\mathrm{c})}{kT}\right)}{(2I_\mathrm{p}+1)\sum(2J+1)\exp\left(-\frac{E_\mathrm{p}(J,K_\mathrm{a},K_\mathrm{c})}{kT}\right)}, \tag{2.25}$$

where I_o and I_p are the total nuclear spin, according to the hydrogen nuclear spins being parallel ($I_\mathrm{o} = 1$, $\uparrow\uparrow$) or anti-parallel ($I_\mathrm{p} = 0$, $\uparrow\downarrow$). The sum in the numerator (denominator) extends over all ortho (para) levels $J_{K_\mathrm{a}K_\mathrm{c}}$ (Mumma et al. 1987), for which $K_\mathrm{a} + K_\mathrm{c}$ = odd (even) for ortho-H_2O (para-H_2O) levels. In Fig. 2.2, the LTE values of the OPRs of H_2 and H_2O are plotted as a function of kinetic temperature. It is found that the OPR in LTE converges towards 3 for H_2 at high temperatures ($T \gtrsim 200$ K), whereas in the case of H_2O the statistical equilibrium value (OPR = 3) is attained at temperatures exceeding ~ 60 K.

2.4.1 Influence of different collisional rate coefficients

Recently, new collisional rate coefficients were presented by Dubernet et al. (2006) using a new interaction potential for the lowest 10 rotational levels of para- and ortho-H_2O in collisions with p- and o-H_2, for kinetic temperatures from 5 K to 20 K. These rate coefficients differ from the ones previously described, especially for collisions with p-H_2. In order to quantify the differences, we model the level populations for water as a two-level molecule in a static cloud with a H_2 density of 10^4 cm^{-3} and a kinetic temperature of 20 K, and compare this with the level populations adopting the

Dubernet & Grosjean (2002) and Grosjean et al. (2003) rates. We find that the population of the upper states differ by up to 60% in the optically thin regime. Note that the rate coefficients for temperatures downwards of 20 K differ even more from the rates presented in Dubernet & Grosjean (2002) and Grosjean et al. (2003), hence an even larger deviation will be found.

2.5 Benchmarking the code

In order to work out a radiative transfer problem, one needs to solve the rate equations (Eq. 2.9). Iterative methods are needed as this set of equations describe a non-linear and non-local problem. Since Bernes (1979), most of the tools used in molecular radiative transfer have been based on one-zone escape probability methods, Monte Carlo techniques, and Λ-iteration schemes for the iterative solution of the non-LTE problem. Eventhough Monte Carlo techniques can cope with complicated geometries, its intrinsic random noise is a major drawback. On the other hand, the Λ-iteration scheme is very easy to implement, but converges slowly in highly optically thick regions. Therefore, this method is extended into an ALI scheme in which the convergence of the level populations is speed up. It has been extensively used in stellar and solar astrophysics and has even been combined with Monte Carlo techniques (Hogerheijde & van der Tak 2000).

Monte Carlo and ALI codes solve the transfer problem in a similar way in that the internal radiation field is computed at any position in the cloud following Eq. 2.5 – 2.6. For this reason it becomes a time consuming task. The calculation of the internal radiation field in the escape probability method is replaced by Eq. 2.10, which depends solely on the escape probabilities. As a result, the computing time can drop, up to a factor of 10 – 100 for the same problem. Consequently, the escape probability method is favoured to solve the radiative transfer in optically thick media.

In order to verify and quantify the accuracy of the code, we have compared it to a number of test problems. In this, a number of different molecules (HCO^+ and H_2O) and a large range of ambient conditions are considered. The following problems are typically encountered in the field of sub-millimeter molecular line modeling. These problems have much of the complicated physics included, such as velocity- and temperature gradients, non-constant line widths, multiple levels etc.

2.5.1 H_2O

To test β3D, we calculate the level populations presented at the water radiative transfer workshop, held in Leiden (2004). Three test problems were presented: a static two-level problem, an expanding two-level problem, and

an asymptotic giant branch (AGB) star with 45-level ortho- and para-H_2O (van der Tak et al. 2005). The first two problems have an analytical solution[1], and are therefore good test problems.

Static cloud

We consider the simple case of a two-level water molecule (1_{10} and 1_{01} states) in an isothermal, constant density sphere for o-H_2O abundances, relative to H_2, of 10^{-10} and 10^{-5}. In these cases, the optical depth increases from ~ 0.1 (optically thin) to 10^4 (optically thick). The parameters used for this model are listed in Table 2.1. Level populations are calculated in a spherical symmetric geometry with 200 radial shells by means of the β3D code as described in Section 2.3. Resulting level populations together with the results of other codes are plotted in Fig. 2.3. The relative differences between the codes are shown in comparison to the mean. The solid lines are the results of the β3D code.

The critical density for this transition is 1.59×10^7 cm^{-3}. However, the effective critical density is reduced due to radiative trapping by a factor in proportion to the escape probability, i.e., $n_{\rm cr,eff} = n_{\rm cr} \times \beta$, with $\beta \sim 1/\tau$ for large τ. Thus, in the high water abundance case, the level populations are driven in the interior towards LTE as the effective critical density drops below the H_2 density. In the outer regions, the upper level populations drop due to the divergence from LTE. In this regime, the difference from the mean value increases from $\sim 5\%$ in the inner regions towards $\sim 10\%$ in the outer regions. In the optically thin case, the results of the β3D code differ by $\sim 3\%$ in the inner radius to $\sim 6\%$ at the outer radius.

Table 2.1: Model parameters for a static cloud

Outer radius	0.1 pc
Inner radius	0.001 pc
H_2 density	10^4 cm^{-3}
Gas temperature	40 K
Velocity dispersion*	0.32 km s^{-1} (FWHM)
De-excitation rate coefficient	2.18×10^{-10} cm^{3}s^{-1}
Excitation rate coefficient	1.12×10^{-10} cm^{3}s^{-1}
No dust or velocity gradient	

* Only thermal broadening, no turbulence.

[1] *http://www.sron.rug.nl/~vdtak/H2O/radxfrtest.pdf*

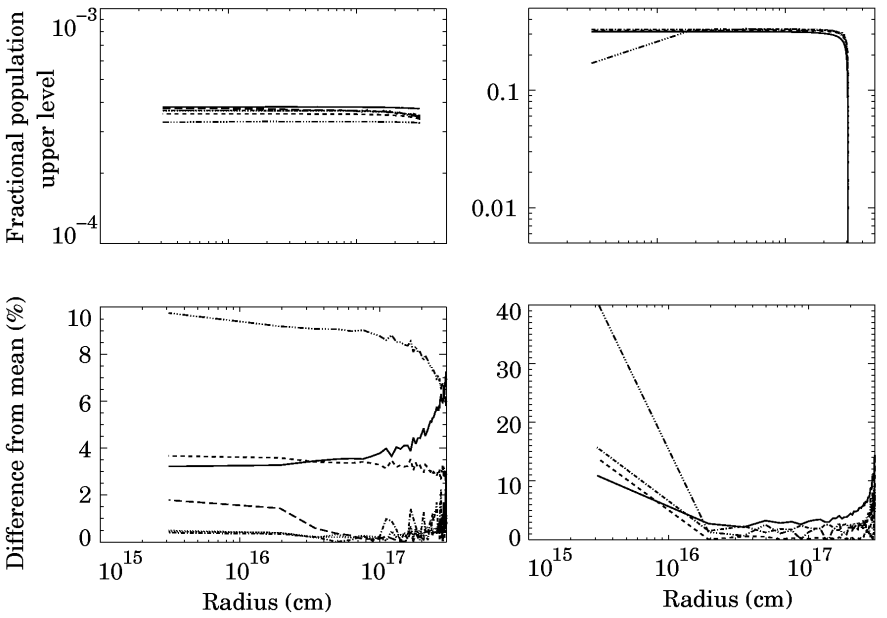

Figure 2.3: *Upper panels:* fractional upper level populations of ortho-H_2O in case of a static two-level problem. The solid line is from the β3D method. *Bottom panels:* difference of the upper level populations with respect to the mean. *Left panels:* $X(H_2O) = 10^{-10}$, *right panels:* $X(H_2O) = 10^{-5}$.

Expanding cloud

We adopt the same excitation and cloud model as in the static case, but add a velocity gradient $V_R = \alpha \times R$, with $\alpha = 100$ km/s/pc. Note that the thermal line width is $\ll V_R(R_{\rm out})$. Resulting level populations together with the results of other codes are plotted in Fig. 2.4. The solid lines are the results of the β3D code.

At small radii, this problem has an analytical solution for the level populations with an upper level population of 5.613×10^{-4} for the high abundance ($X(H_2O) = 10^{-8}$, $\tau \sim 1$), and a population of 3.250×10^{-4} for the low abundance ($X(H_2O) = 10^{-10}$, $\tau \sim 10^{-2}$) case. These values are based on the Sobolev approximation, relevant in regions undergoing a large velocity gradient (LVG). Since the Sobolev method takes into account only local effects, this method is solely suitable for regions where $\tau \ll 1$. After all, the continual process of absorption and re-emission causes photons to wander all over the source, and a local escape factor can only be a rough approximation at best. This can be seen in Fig. 2.4, where all the codes agree with the analytical solution in the low abundance case. In the case of a water

abundance of 10^{-8}, the optical depth $\tau \sim 1$. Since the Sobolev approximation is applicable for regions where $\tau \ll 1$, the result found with the β3D code differs slightly from the analytical solution. Note that the upper level population computed with the β3D method approaches this value closely without any noise, in contrast to other codes, within $\sim 10\%$ of the analytical value. Some codes indicate even a decrease, which is an artifact of gridding the velocity field along with the temperature and the density, hence underestimating the effective optical depth along a line of sight.

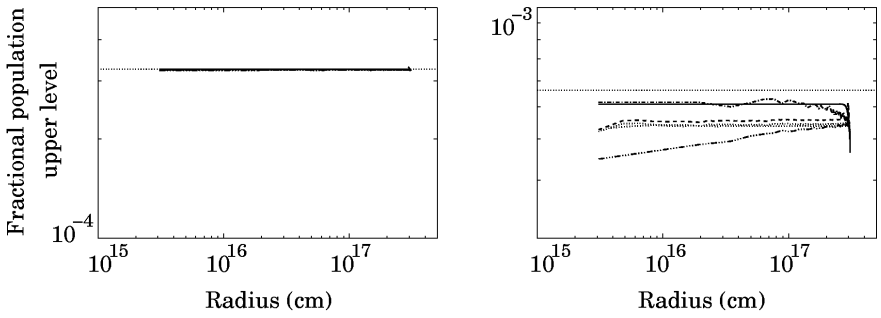

Figure 2.4: Fractional upper level populations of ortho-H_2O in case of an expanding sphere for H_2O. *Left panel*: $X(H_2O) = 10^{-10}$, *right panel*: $X(H_2O) = 10^{-8}$. The horizontal dotted line indicates the analytical solution.

2.5.2 HCO^+

A more realistic test problem is based on a model by Rawlings et al. (1992, 1999) to analyze HCO^+ data for an infalling envelope around a protostar. This problem was presented at a workshop held in Leiden (1999) to compare line radiative transfer programs. Results of that campaign are written down in van Zadelhoff et al. (2002). The model describes how the cloud core collapses from the inside-out. The model is similar to the analytical inside-out collapse model by Shu (1977), but includes more realistic physics. Figure 2.5 shows the structure of the cloud at a particular time during the collapse phase. This is the input of the model for our test case. The collapse can clearly be seen in the radial velocity, which is 0 for radii larger than 10^{17} cm, and directed towards the source for smaller radii. The density profile is given by a power-law of the form $n(r) = n_0(r/r_0)^m$, where $m = -1.5$ inside the collapsing sphere ($r < 10^{17}$ cm) and $m = -2.0$ outside. The model parameters are specified at 50 radii, logarithmically spaced between 10^{16} and 4.6×10^{17} cm. Resulting level populations together with the results of other codes are plotted in Fig. 2.6. The relative differences between

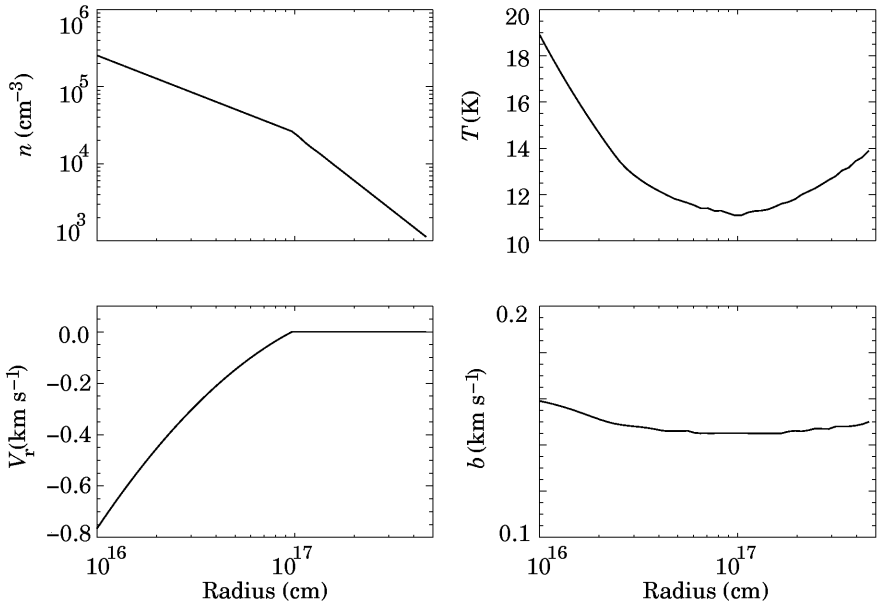

Figure 2.5: Physical structure of the test model to analyze HCO^+ data for an infalling envelope around a protostar. *Upper left*: density; *lower left*: radial velocity; *upper right*: temperature; *lower right*: turbulent line width b. Changes in the density and velocity distribution are seen at the point where infall starts. The temperature of the gas at the inside rises due to the infall, while the outside is heated by the interstellar radiation field (van Zadelhoff et al. 2002).

the codes are also shown in comparison to the mean. The solid lines are the results of the β3D code.

The resulting level populations of the β3D code are consistent with the other codes. For level $J = 1$, the differences with respect to the mean are in the optically thin and thick regime only a few per cent. These differences increase in both cases up to a few 10% for the $J = 4$ level. However, note that the bulk of the level populations, i.e., 99.7%, is in the ground state levels.

The level populations can be used to calculate the emergent intensity of different transitions through Eq. (2.20) – (2.22). In the case of an optically thin line, the intensity scales linear with the level populations. Thus, a 10% difference in the level populations between the different codes results in intensities that differ 10%. However, when a line is optically thick, the intensities can differ by smaller factors than the level populations.

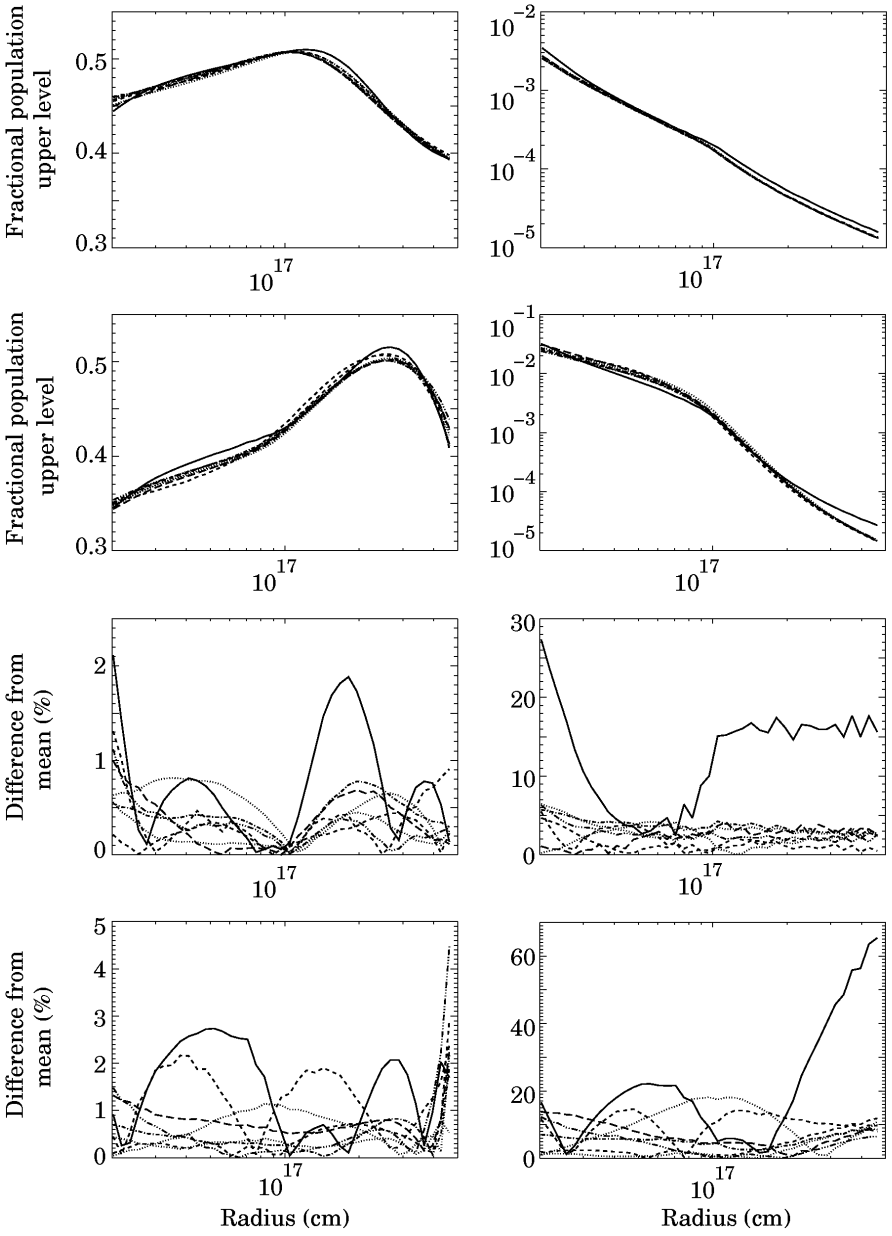

Figure 2.6: Fractional level populations of the $J=1$ (*left panels*) and $J=4$ level (*right panels*) of HCO^+. *Upper panels*: $X(HCO^+)=10^{-9}$, *bottom panels*: $X(HCO^+)=10^{-8}$.

2.5.3 Conclusions

In this chapter, a newly developed radiative transfer code is described and tested. The main advantages of the program are its speed and dimensionality. Together, it allows the user to solve a more complicated problem unlimited to any symmetry assumption. Although applicable for any atom and molecule, e.g., HCN, HNC, CO, CN, CS, HCO^+, ..., the code is extremely suitable for atoms and molecules that emit in the NIR-mm region, i.e., rotational and ro-vibrational transitions. Furthermore, the excitation by dust emission, particularly important for water, is included in full. It is shown that the results found with β3D overlap the outcome of already existing Monte Carlo and ALI codes. We therefore believe that the code is an exquisite tool to use in preparatory work for and future data of Herschel and ALMA, as well as in the analysis/interpretation of already exisiting data.

Acknowledgements

We are grateful to Gerd-Jan van Zadelhoff and Floris van der Tak for making the results of the participating radiative transfer codes available as presented on the workshops held in Leiden.

References

Bernes, C. 1979, A&A, 73, 67
Castor, J. I. 1970, MNRAS, 149, 111
Chrysostomou, A., Brand, P. W. J. L., Burton, M. G., & Moorhouse, A. 1993, MNRAS, 265, 329
de Jong, T., Chu, Shih-I, & Dalgarno, A. 1975, ApJ, 199, 69
de Jong, T., Boland, W., & Dalgarno, A. 1980, A&A, 91, 68
Dubernet, M.-L., & Grosjean, A. 2002, A&A, 390, 793
Dubernet, M.-L., Daniel, F., Grosjean, A. et al. 2006, A&A, 460, 323
Elitzur, M. 1992, Astronomical masers (Astronomical masers Kluwer Academic Publishers (Astrophysics and Space Science Library. Vol. 170), 365 p.)
Elitzur, M., & Asensio Ramos, A. 2006, MNRAS, 365, 779
Faure, A., Gorfinkiel, J. D., & Tennyson, J. 2004, MNRAS, 347, 323
Federman, S. R., Glassgold, A. E., Jenkins, E. B., & Shaya, E. J. 1980, ApJ, 242, 545
Green, S., Maluendes, S., & McLean, A. D. 1993, ApJS, 85, 181
Goldreich, P., & Kwan, J. 1974, ApJ, 189, 441
Grosjean, A., Dubernet, M.-L., & Ceccarelli, C. 2003, A&A, 408, 1197
Hasegawa, T., Gatley, I., Garden, R. P., et al. 1987, ApJ, 318, L77
Helmich, F. P., van Dishoeck, E. F., Black, J. H., et al. 1996, A& A, 315, L173
Herpin, F., & Cernicharo, J. 2000, ApJ, 530, L129
Hogerheijde, M. R., & van der Tak, F. F. S. 2000, A&A, 362, 697
Hogerheijde, M. R., van Dishoeck, E. F., Blake, G. A., & van Langevelde, H. J. 1998, ApJ, 502, 315
Hora, J. L., & Latter, W. B. 1996, ApJ, 461, 288
Hummer, D. G. 1968, MNRAS, 138, 73
Hummer, D. G., & Rybicki, G. 1970, MNRAS, 150, 419

Kaufman, M. J., & Neufeld, D. A. 1996, ApJ, 456, 611
Ladd, E. F., Fuller, G. A., & Deane, J. R. 1998, ApJ, 495, 871
Meijerink, R., Spaans, M., & Israel, F. P. 2007, A&A, 461, 793
Mumma, M. J., Weaver, H. A., & Larson, H. P. 1987, A&A, 187, 419
Neufeld, D. A., & Kaufman, M. J. 1993, ApJ, 418, 263
Neufeld, D. A., & Melnick, G. J. 1991, ApJ, 368, 215
Ossenkopf, V., & Henning, T. 1994, A&A, 291, 943
Phillips, T. R., Maluendes, S., & Green, S. 1996, ApJS, 107, 467
Poelman, D. R., & Spaans, M. 2005, A&A, 440, 559
Ramsay, S. K., Chrysostomou, A., Geballe, T. R., Brand, P. W. J. L., & Mountain, M. 1993, MNRAS, 263, 695
Schöier, F. L., van der Tak, F. F. S., van Dishoeck, E. F., & Black, J. H. 2005, A&A, 432, 369
Shupe, D. L., Larkin, J. E., Knop, R. A., et al. 1998, ApJ, 498, 267
Sobolev, V. V. 1960, Moving envelopes of stars. Harvard University press, Cambridge
Spaans, M. 1996, A&A, 307, 271
Spaans, M., & van Langevelde, H. J. 1992, MNRAS, 258, 159
Stark, R., Sandell, G., Beck, S. C., et al. 2004, ApJ, 608, 341
van der Tak, F., Neufeld, D., Yates, J., et al. 2005, in the Dusty and Molecular Universe: A Prelude to Herschel and ALMA, ed. A. Wilson, 431
van Dishoeck, E. F. 2004, ARA&A, 42, 119
van Zadelhoff, G.-J., Dullemond, C. P., van der Tak, F. F. S., et al. 2002, A&A, 395, 373